Optics and Laser Technology 97 (2017) 308–315

Contents lists available at ScienceDirect

Optics and Laser Technology

journal homepage: www.elsevier.com/locate/optlastec

Full length article

Effect of laser shock processing on fatigue life of 2205 duplex stainless steel notched specimens

César A. Vázquez Jiménez [a,*], Gilberto Gómez Rosas [b], Carlos Rubio González [c], Vignaud Granados Alejo [c], Silvina Hereñú [d]

[a] Posgrado en Ciencia de Materiales, Centro Universitario de Ciencias Exactas e Ingenierías, Universidad de Guadalajara, Blvd. Marcelino García Barragán 1421, Guadalajara, Jal. 44430, Mexico
[b] Departamento de Física, Centro Universitario de Ciencias Exactas e Ingenierías, Universidad de Guadalajara, Blvd. Marcelino García Barragán 1421, Guadalajara, Jal. 44430, Mexico
[c] Centro de Ingeniería y Desarrollo Industrial, Pie de la cuesta 702, Desarrollo San Pablo, Querétaro, Qro. 76130, Mexico
[d] Instituto de física Rosario, Bv. 27 de febrero 210 bis (2000) Rosario, Santa Fe, Argentina

A R T I C L E I N F O

Article history:
Received 23 December 2016
Received in revised form 10 July 2017
Accepted 17 July 2017

Keywords:
Laser shock processing
Fatigue test
Duplex stainless steel
Residual stress
Microhardness
Rolling direction

A B S T R A C T

The effect laser shock processing (LSP) on high cycle fatigue behavior of 2205 duplex stainless steel (DSS) notched samples was investigated. The swept direction parallel (LSP 1) and perpendicular (LSP 2) to rolling were used in order to examine the sensitivity of LSP to manufacturing process since this steel present significantly anisotropy. The Nd:YAG pulsed laser operating at 10 Hz frequency and 1064 nm wavelength was utilized. The LSP configuration was the water jet mode without protective coating. Notched specimens 4 mm thick were treated on both sides, and then fatigue loading was applied with $R = 0.1$. The results showed that the LSP 2 condition induces higher compressive residual stresses as well as a higher fatigue life than the LSP 1 condition. By applying LSP 2 condition, an enhancement of fatigue life up to 402% is reported. In addition, the microhardness profiles showed different depths of hardening layer for each direction, according to the anisotropy observed.

1. Introduction

In industrial components, a lot fatigue failures appear near a discontinuity [1–8], either accidentally due to the machining (grooves, indentations or surface marks) generated during operation of the workpiece (by wear, impact, etc.) or imposed by the design of a mechanical component while binding or interacting with another (grooves, holes, threads, keyways, fillets, etc.). These discontinuities are preferential areas for nucleation of a crack due to high stress concentration generated in adjacent areas. The processes that generate compressive residual stresses can be beneficial and prolong fatigue life in metallic materials [9–12]. The LSP treatment is based on the induction of a field of residual compressive stresses through the propagation of shock waves at high pressure on the material surface [13]. This technique allows to treat specific areas by programming of laser impacts on critical areas of stress concentration in mechanic components to reduce the high probability of failure that characterize these geometries. Stress concentrators like open holes [14–18] and notches [19–21], have reported significant improvements increasing in limit resistance to fatigue and the number of cycles to failure by applying LSP treatment. However not all cases have proved beneficial, in some materials, LSP treatment has deteriorated fatigue properties [22,23].

It is known that the LSP treatment has proven to be an effective technique to improve fatigue resistance in various metal alloys. However, the fatigue behavior may vary depending on the type of stress concentrator and the material, which makes necessary to characterize this behavior for alloys with high impact in different industrial sectors. The 2205 DSS has various industrial applications (offshore platforms, power plants, desalination plants and gas gathering) in components submitted to cyclic loads in corrosive environments. Different properties of 2205 DSS have been studied by applying LSP treatment, such as the change in fatigue crack growth rate [24], abrasive wear and corrosion resistance [25], and hardness [26,27], obtaining significant improvements in all cases. However, no previous work has been reported to evaluate the effect of LSP in fatigue resistance of 2205 DSS with stress concentrators. The objective of this paper is dual; first is to analyze the effect of LSP treatment on high cycle fatigue behavior of 2205 DSS in notched specimens and also evaluate the effect of LSP swept orientation with respect to rolling direction since this steel presents a

* Corresponding author.
E-mail address: vazquez_cesar@ucol.mx (C.A. Vázquez Jiménez).

http://dx.doi.org/10.1016/j.optlastec.2017.07.020
0030-3992/

significant anisotropy. Residual stress distribution and microhardness profiles are determined by hole drilling method and Vickers indentation, respectively. In addition, the fracture surface is analyzed by scanning electron microscope (SEM).

2. Material and methods

The specimens were obtained from a plate of 2205 DSS with 9.5 mm thickness. The chemical composition of 2205 DSS analyzed by spark emission spectrometer is listed in Table 1. The mechanical properties of the samples were determined by tensile test using dog-bone type specimens. The offset tensile yield stress is 520 MPa, ultimate tensile strength is 710 MPa and elastic modulus is 190 GPa. The microstructure of 2205 DSS is shown in Fig. 1. The austenite phase (light color) is distributed inside the ferritic phase matrix (dark color). This steel presents a significant anisotropy, the rolling direction (Fig. 1a) shows a higher elongation of austenite phase in comparison with the perpendicular direction (Fig. 1b).

The specimens for fatigue tests were cut with a waterjet machine at high pressure to minimize the thermal damage and roughness along the cut surface, then the thickness was reduced by CNC to 4 mm and finally the machining marks were erased with a surfaces grinding, leaving a finish surface of 0.1 μm in the longitudinal axis direction of the sample (rolling direction and loading axis). Through optical observation it was corroborated that the anisotropy of the phases morphologies does not change along the thickness. The dimensions of the specimens are shown in Fig. 2. The fatigue tests were performed on a MTS810 servo-hydraulic system at room temperature in the air. All specimens were tested in tension-tension (axial) fatigue at a 20 Hz frequency, a $R = 0.1$ stress ratio and a maximum applied stress was between 275 and 300 MPa. The fracture surface was analyzed by SEM microscopy.

Vickers microhardness measurements were performed over the parallel and perpendicular direction to rolling of each material condition (untreated, LSP 1 and LSP 2). The Vickers indentations were performed with a load of 200 g during 10 s. With these results thereafter, the microhardness profiles were obtained.

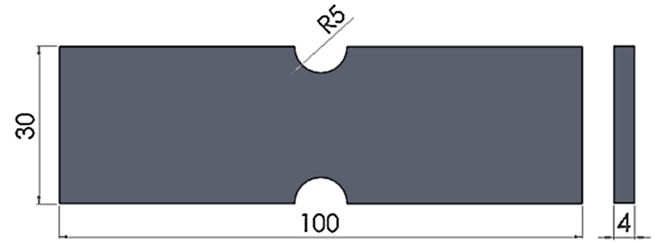

Fig. 2. Dimension of samples for fatigue tests (mm).

Residual stress distribution was determined by the hole drilling method according to the ASTM standard E837-01 [28]. Strain gages rosettes EA-13-062RE-120 along with a RS-200 Milling Guide from Measurements Group were used. The samples were prepared with the same surface finish as the fatigue specimens and the measurements were performed in the center of the sample as shown in Fig. 3.

The experimental array of LSP treatment is shown in Fig. 4. It consists of a Q-switched Nd:YAG pulsed laser, Quantel Brilliant b model, operating at 10 Hz with a wavelength of 1064 nm. The pulse duration (FWHM) was 6 ns. The laser beam is deflected by a mirror and focused by lens to deliver 0.85 J per pulse in 1 mm diameter (spot size) onto the target surface with a fluence of 108.2 J/cm^2. The plasma is formed when the interaction between the laser pulse and the material surface occurs as illustrated in Fig. 5. A thin layer of water (~2 mm) is used to confine the plasma during expansion, increasing the pressure on the material surface in the order of GPa. This pressure, leads to shock waves formation, which propagates into the material inducing a compressive

Table 1
Chemical composition of 2205 DSS.

Element	C	Si	Mn	P	Cr	Mo	Ni	N
wt (%)	0.021	0.42	1.22	0.028	22.13	3.08	5.56	0.188

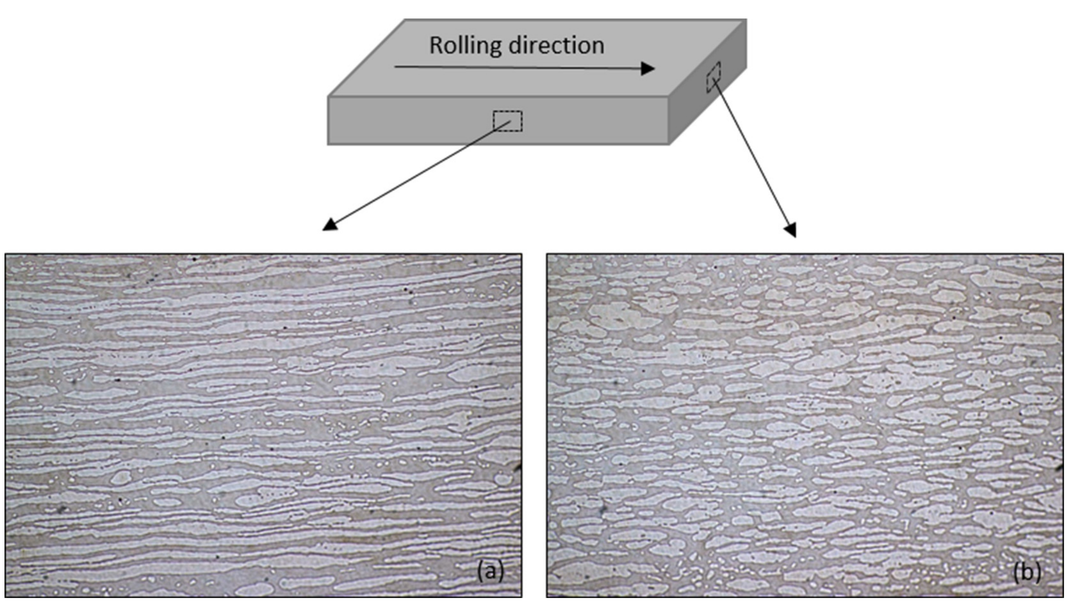

Fig. 1. Microstructure of 2205 DSS: (a) parallel to rolling and (b) perpendicular to rolling.

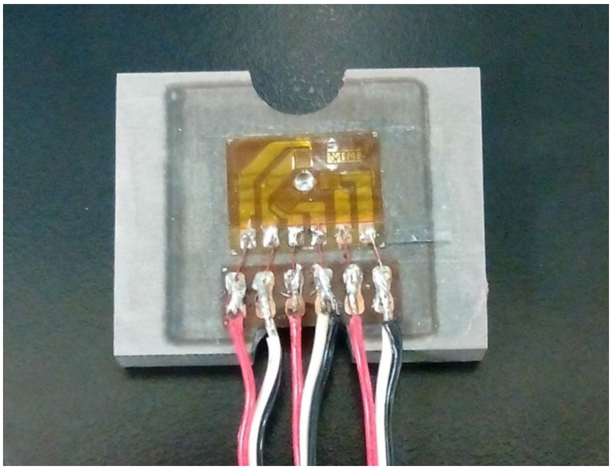

Fig. 3. Specimens for residual stress measurements.

residual stress field due to the plastic deformation of the treated sample. A motorized *x-y* system with 0.1 μm of resolution and maxim velocity of 2.5 mm/s was utilized to guide the path of the impacts (swept direction) in the treatment zone. The pulses density used for these experiments was 2500 pulses/cm^2. This parameter is determined by controlling the motors speed. The treatment modality used was without ablative layer [29].

The LSP treatment is applied in an area of 2.5 × 2.5 cm on both sides of the fatigue test specimen. Two swept directions of LSP treatment were applied: (a) parallel to rolling direction (LSP 1) and (b) perpendicular to rolling direction (LSP 2), as shown in Fig. 6.

3. Results and discussion

3.1. Microhardness

The microhardness profiles comparison for untreated and treated samples is shown in Fig. 7. The microhardness of untreated material takes a constant value of approximately 290 HV along the parallel direction to rolling (Fig. 7a). The microhardness profiles for both LSP conditions are similar. The maximum value obtained was 360 HV at a depth of 100 μm, corresponding to increases of 24%, then drop gradually to the microhardness of untreated material around a depth of 300 μm. For the perpendicular direction to rolling (Fig. 7b), the microhardness of untreated material takes a constant value of approximately 260 HV. In this direction, both LSP conditions also present similar microhardness profiles. The maximum value obtained was 360 HV at a depth of

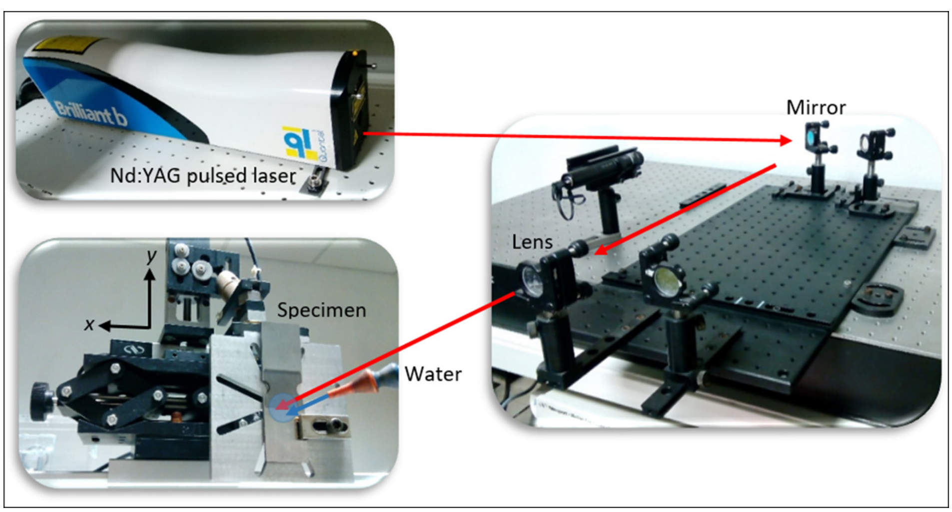

Fig. 4. Experimental set-up of LSP.

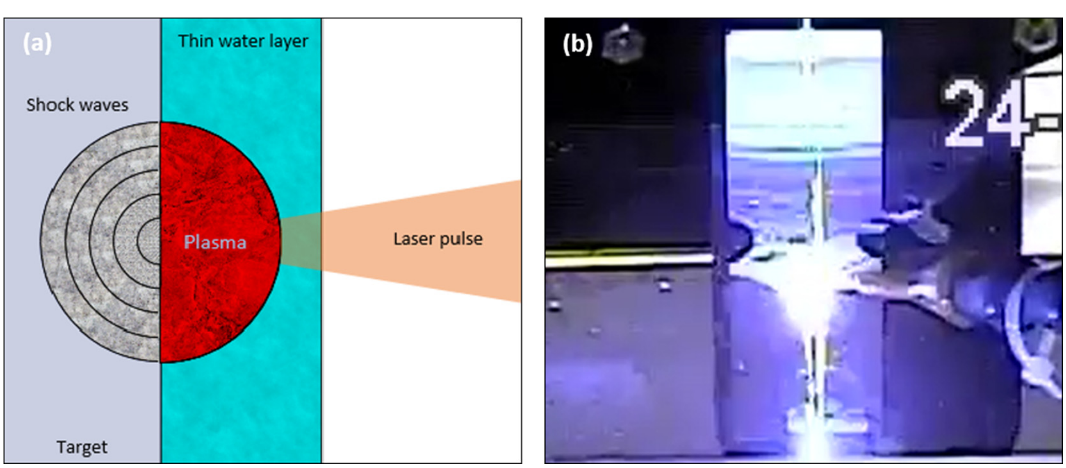

Fig. 5. Principle of LSP: (a) Schematic and (b) Real sample during LSP treatment.

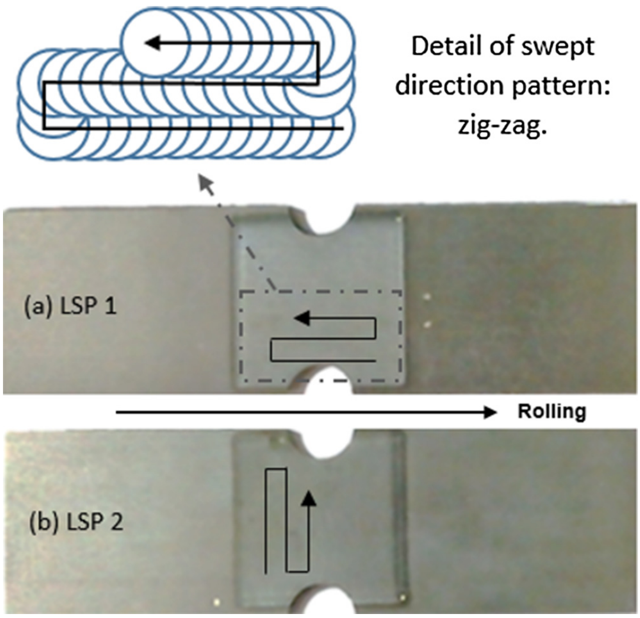

Fig. 6. Specimens for fatigue test: (a) LSP 1: swept direction parallel to rolling, (b) LSP 2: swept direction perpendicular to rolling.

100 μm, corresponding to 38.5% improvement, then drop gradually to the microhardness of untreated material around a depth of 500 μm. It is found that the untreated material presents a slight increase of microhardness in the parallel direction to rolling, this can be attributed to more compact and elongated phases distribution as a consequence of rolling process [30,31]. However, the benefit of the LSP treatment is that it increases the hardness and eliminates anisotropy in near-surface (360 HV in both directions).

E. Castañeda [26], reported an increase in near-surface microhardness of 12% with similar LSP parameters (0.85 J pulse energy, 6 ns pulse duration, 1.5 mm spot diameter and 2500 pulses/cm^2) in 2205 DSS. However, this microhardness increase is lower than that found in the present work. This fact could be attributed to the smaller spot size (1 mm) which produces a higher energy per unit area. H. Lim [27], reports a similar microhardness increase in 2205 DSS using ablative layer during LSP treatment.

3.2. Residual stress

The residual stress distribution of untreated material with respect to the depth is shown in Fig. 8. A tensile stress is observed. The maximum tensile stress in the rolling direction (Sxx) is 475 MPa at a depth of about 0.25 mm, while the maximum tensile stress in the perpendicular direction to rolling (Syy) is 260 MPa corresponding to the same depth. It is observed that the residual stresses do not tend to equilibrium itself in the first millimeter of depth. However, with the equipment available it was only possible to perform the measurements up to this depth. The anisotropy shown in residual stress components can be attributed to different phase morphologies in each direction and therefore, different strain level induced by the rolling process [32].

The residual stress distribution as a function of depth with LSP1 treatment condition is shown in Fig. 9, in which a compressive residual stress state induced by LSP treatment is observed. The maximum compressive stress in the rolling direction (Sxx) is 510 MPa at a depth of about 0.4 mm, while the maximum compressive stress in the perpendicular direction to rolling (Syy) is 700 MPa corresponding to the same depth. A smaller Sxx component is observed; Correa et al. [33] explains the anisotropy in the compressive residual stresses distribution induced by treatment LSP treatment through overlapping and the swept direction effects by simulating impacts using the finite element method. It has been found the stress component perpendicular to swept direction is greater than the parallel component. Similar observations have been reported for different metal alloys [34,35].

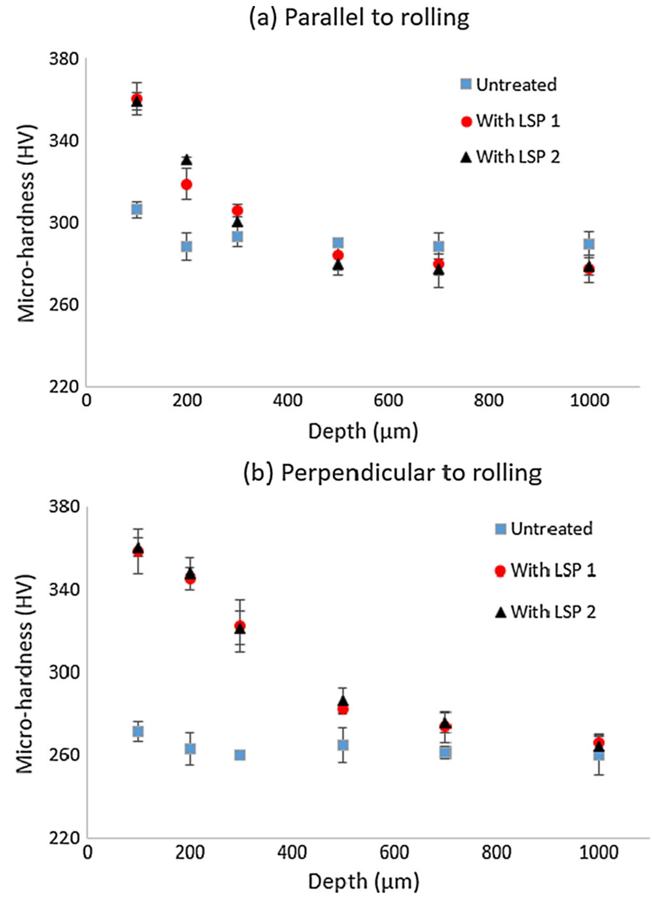

Fig. 7. Micro-hardness profile in both directions: (a) parallel and (b) perpendicular to rolling.

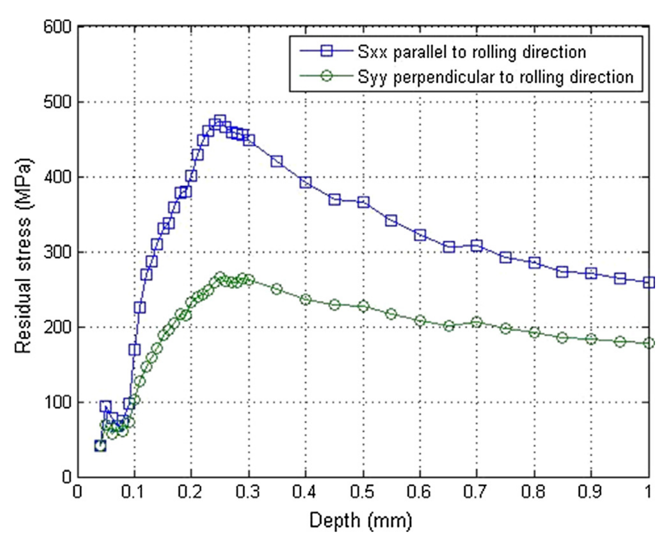

Fig. 8. Residual stress distribution of untreated material.

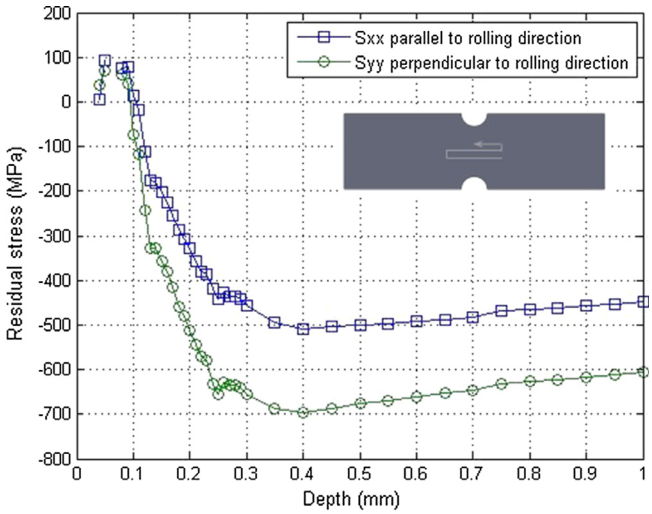

Fig. 9. Residual stress distribution of LSP1 treatment condition.

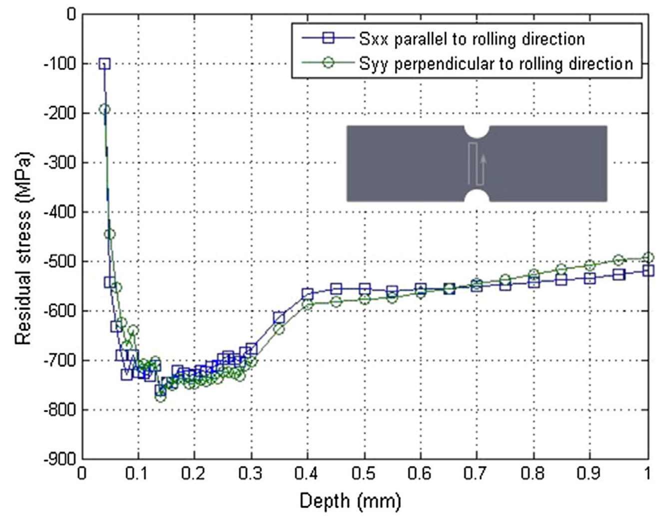

Fig. 10. Residual stress distribution of LSP2 treatment condition.

The residual stress distribution as a function of depth with LSP2 treatment condition is shown in Fig. 10 in which a compressive residual stresses state is also observed. The maximum compressive stress in the rolling direction (Sxx) is 770 MPa at a depth of about 0.14 mm, while the maximum compressive stress in the perpendicular direction to rolling (Syy) is 780 MPa corresponding to the same depth. The residual stress distribution is modified with this LSP configuration. It can be attributed to the effect of the swept direction with respect to the rolling orientation. The LSP 2 condition produces on the 2205 DDS a significant decrease in the anisotropy of the residual stress field and higher compressive residual stress values with respect to the effect generated by the LSP 1 condition.

3.3. Fatigue test

Fatigue life results are shown in Fig. 11. Considering the fatigue life of untreated specimen as the reference, in both LSP conditions an increase of fatigue life is observed. The best improvement is given by LSP2 condition. It can be observed that LSP2 condition lasted 889,900 cycles to failure corresponding to 79% improvement with respect to untreated specimens (496,500 cycles to failure). While LSP1 condition lasted 669,000 cycles to failure corresponding to 35% improvement.

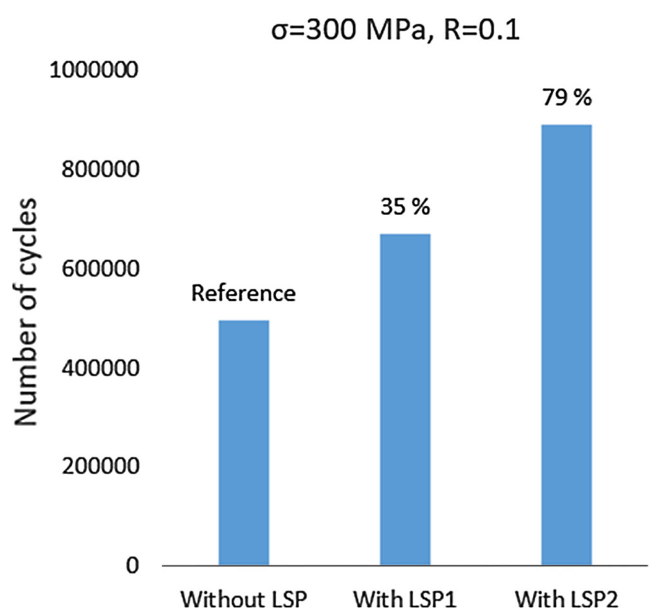

Fig. 11. Fatigue properties comparison with different swept directions.

C. Correa et al. [36] investigated the effect of the swept direction on the fatigue life of 316 L stainless steel alloy. Contrary to the results displayed in the present DSS, these authors reported that improvement of fatigue life was observed when the swept direction is parallel to the specimen longitudinal axis. In this regard, factors such as tensile residual stresses in the mid-thickness (due to equilibrium of stress state) and residual stresses induced at the sample edges [37,38] are ascribed to have a high influence on the fatigue life. Additionally, the LSP patterns should also be taken into account. Spiral and zig-zag type swept directions were compared in Al 6061-T6 by A. Salimianrizi [34]. The maximum surface hardness was obtained with the spiral-type swept direction. Alternatively, C. Correa [33] proposes a random type swept pattern, which achieves a significant decrease the residual stresses anisotropy in comparison with zig-zag swept pattern. Therefore, though the anisotropy of induced residual stress by LSP has been studied in relation to swept direction and the pulses sequence, no work was found considering the material's microstructural anisotropy. In this work, it is evidenced that the material's microstructural anisotropy caused by rolling also affects the distribution of induced residual stresses and consequently changes the fatigue behavior. It is well known that in DSS microstructural features including chemical composition, volume fraction of phases, phase distribution, grain size and heat treatment influence short crack initiation and growth. During a fatigue test, the amount of plastic deformation each phase bears depends on the elastoplastic properties and the load sharing between austenite and ferrite [39] In this respect, attempting to have a more complete understanding between the residual stress anisotropy and microstructure, future work will analyze other microstructural features such as dislocation structure and grain size.

Two more fatigue tests were performed with LSP-2 condition. The results are shown in Fig. 12. When the maximum applied stress was 287.5 MPa, fatigue lives were 456,600 and 623,000 cycles to failure for untreated specimens, and 2,128,500 cycles to failure for LSP treated specimens, corresponding to an average improvement of 294%. When the maximum applied stress was 275 MPa, fatigue life was 836.700 cycles to failure for untreated specimen, while the LSP treated specimen reached 4,200,000 cycles

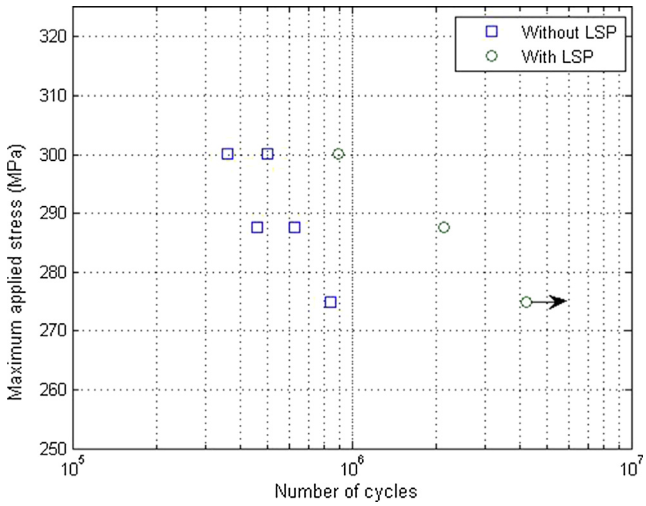

Fig. 12. Fatigue test results for LSP2.

without presenting fracture; this point is indicated by an arrow in Fig. 12. Up to this point an improvement up to 402% is achieved by LSP. It can be see that as the maximum stress is decreased on the fatigue test fatigue life is significantly increased on specimens treated by LSP.

Fatigue life is associated with the accumulation of plastic deformation in regions localized (crystalline defects), which, after several loading cycles gives rise to the crack incubation. The compressive residual stresses induced by LSP inhibit the effect of external force and decreases the strain magnitude in the region near surface. Likewise, the increase in hardness, delay the process of fatigue crack initiation in theses vulnerable regions. Thus, both the presence of compressive residual stresses and the increase in surface hardness, result in a significant increase in fatigue life of 2205 DSS.

4. Fracture surface

Figs. 13 and 14 shows aspects of fracture surface of untreated and treated specimens, respectively, at 287.5 MPa stress ampli-

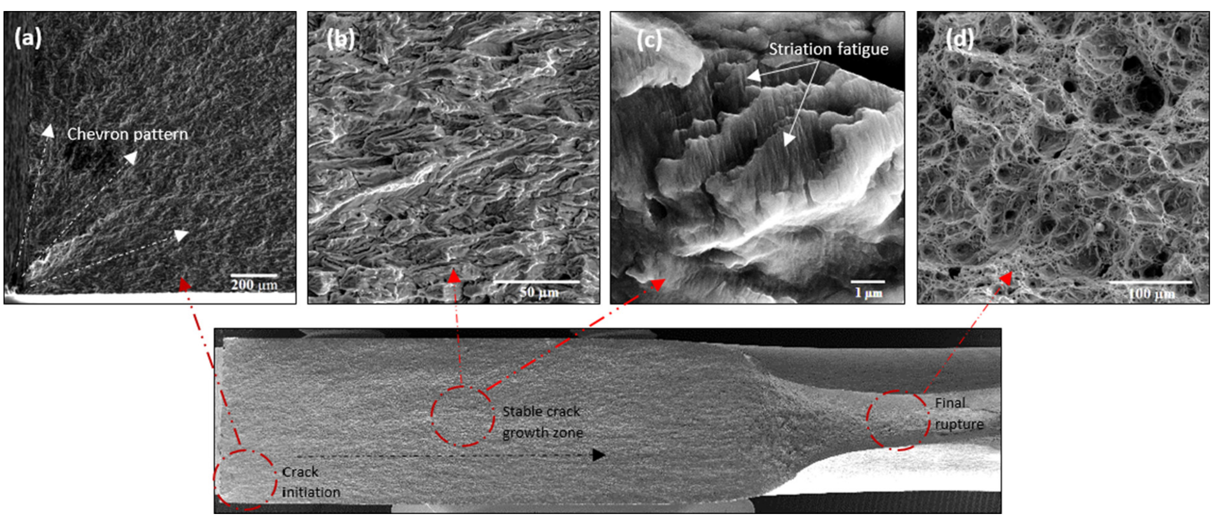

Fig. 13. Fracture surface of specimen without LSP: (a) crack initiation, (b) crack growth, (c) fatigue striation and (d) final rupture.

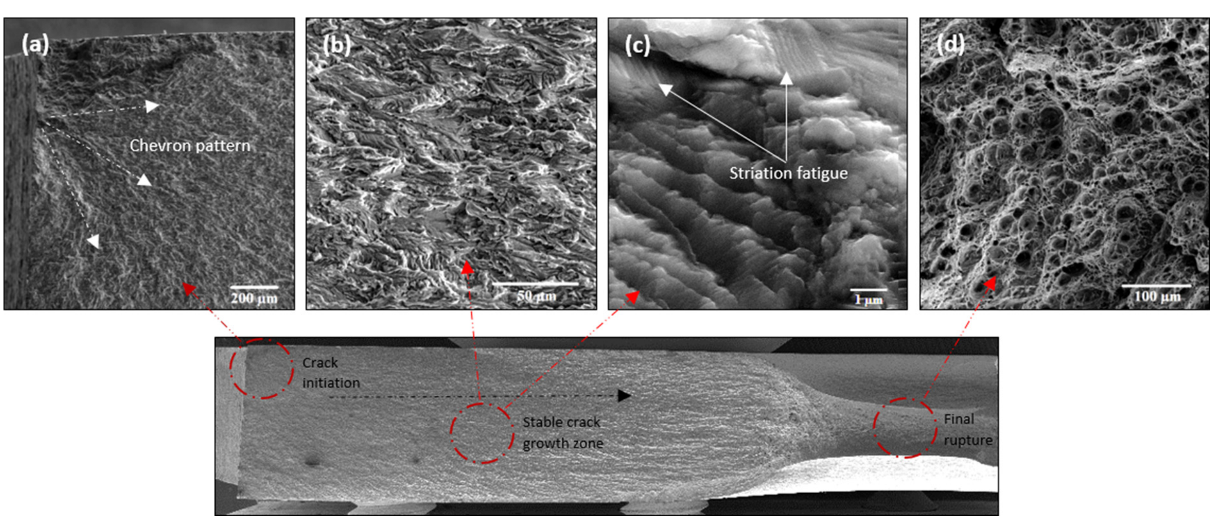

Fig. 14. Fracture surface of specimen with LSP: (a) crack initiation, (b) crack growth, (c) fatigue striation and (d) final rupture.

tude. The crack initiation in the untreated specimen (Fig. 13a) occurs near-surface (~50 μm). While for treated specimen (Fig. 14a) occurs 400 μm below the surface. The shift observed is attributed to hardening layer induced near surface by LSP treatment, which increases the resistance to fatigue crack nucleation and decreases the probability that the crack starts at the surface. This effect has also been observed by Zhang [40,41] and Ren [42] in different aluminum alloys and Hongchao [43] in Ti17 titanium alloy.

Figs. 13b and 14b show the appearance of fracture surface of treated and untreated specimens respectively, at stable crack growth zone. It can be observed in both cases that there is no change in the morphology; the high plastic deformation can be attributed to the high ductility of DSS 2205 (50% deformation). In the same region, the fatigue striation is shown in Figs. 13c and 14c for untreated and treated specimens respectively. In general, the fatigue striation spacing may have different values in different zones along the cross section, and striation are not completely regular. It can be noted that an average fatigue striation spacing of 0.20 μm in both cases. Finally, for final rupture region, in Figs. 13d and 14d similar sizes of dimples and significant thickness reduction are observed corresponding to a ductile failure mechanism. From these figures, it is evident that the LSP influences the crack initiation. This fact can be rationalized by the stability of induced compressive residual stresses. As a long as the stress applied by external load is less than the magnitude of the induced residual stress, the effect of the LSP treatment has a great influence on the fatigue behavior [44]. Once the crack starts and increases in length, the area of the cross section decreases. When the area is sufficiently small, the elastic limit is exceeded and high cyclic plastic deformations are experienced inhibiting the effect of the residual stresses induced by the LSP. This is the reason why the same morphology is observed in the final rupture zone and its surrounding regions in untreated and treated samples.

5. Conclusions

A study was conducted on 2205 DSS notched samples treated with LSP, using two different swept directions: parallel and perpendicular to rolling direction. The effect of LSP treatment on microhardness, residual stress, fatigue life, and fracture surface morphology were characterized. The following conclusions can be drawn:

- By applying the LSP treatment, microhardness near-surface can be increased by 24 and 38.5% for the parallel and perpendicular direction to rolling, respectively. The perpendicular direction to rolling presents a greater hardened layer induced by LSP than the parallel direction to rolling. This can be attributed to different morphology of phases and therefore, different deformation capacity for each direction during LSP treatment.
- It has been shown experimentally that LSP treatment for both swept direction (parallel and perpendicular to rolling direction) eliminates the tensile residual stress due to manufacturing processes and induces high level compressive residual stress with different distribution for each direction according to anisotropy observed in 2205 DSS.
- It has been demonstrated that the LSP treatment is an effective technique for improving fatigue life in notched specimens of 2205 DSS. By setting the swept direction perpendicular to rolling direction, the increase of fatigue life achieves a value of 79% at 275 MPa of stress amplitude, while with the swept direction parallel to rolling direction; the fatigue life improvement is only 35% at the same stress level.
- It has been demonstrated experimentally that the best treatment condition to improve fatigue life was the swept direction perpendicular to rolling direction. In this treatment condition, for values of stress amplitudes between 275 and 300 MPa, an enhancement of 79% up to 402% was obtained.
- The fracture surface morphology is not modified by LSP treatment. No changes were found in fatigue striation and final rupture surface. Only preferential fatigue crack initiation zone was changed from the surface at inward surface due to hardened layer induced near surface by LSP treatment.
- In this paper, sensitivity of LSP to manufacturing processes such as rolling is evidenced. The rolling direction is considered to optimize fatigue life of DSS 2205 by LSP treatment. This optimization can be applied in other properties of DSS 2205 and different metal alloys.

Acknowledgement

The authors thank to Institute of Physics Rosario-Argentina-PICT-2013-1105, CONACYT, CIDESI and University of Guadalajara (Mexico) for their support in the realization of this work.

References

[1] Yue-Yue Ma, Shi Yan, Zhen-Guo Yang, Guo-Shui Qi, Xin-You He, Failure analysis on circulating water pump of duplex stainless steel in 1000 MW ultra-supercritical thermal power unit, Eng. Failure Anal. 47 (2015) 162–177.
[2] S. Griza, M. Reis, Y. Reboh, A. Reguly, T.R. Strohaecker, Failure analysis of uncemented total hip stem due to microstructure and neck stress riser, Eng. Failure Anal. 15 (2008) 981–988.
[3] H. Mohammed Mohsin Ali, Mohamed Haneef. Analysis of fatigue stresses on connecting rod subjected to concentrated loads at the big end. Mater. Today: Proceedings 2015; 2: 2094-2103.
[4] Mile Savkovic, Milomir Gašic, Dragan Petrovic, Nebojša Zdravkovic, Radmila Pljakic, Analysis of the drive shaft fracture of the bucket wheel excavator, Eng. Failure Anal. 20 (2012) 105–117.
[5] P. Roffey, Case study: failure of a high nitrogen stainless steel femoral stem, Eng. Failure Anal. 20 (2012) 173–182.
[6] Borut Zorc, Ales Nagode, Borut Kosec, Ladislav Kosec, Elevator chain wheel shaft break analysis, Case Stud. Eng. Failure Anal. 1 (2013) 115–119.
[7] M.N. Ilman, R.A. Barizy, Failure analysis and fatigue performance evaluation of a failed connecting rod of reciprocating air compressor, Eng. Failure Anal. 56 (2015) 142–149.
[8] O.A. Zambrano, J.J. Coronado, S.A. Rodríguez, Failure analysis of a bridge crane shaft, Case Stud. Eng. Failure Anal. 2 (2014) 25–32.
[9] Charles S. Montross, Tao Wei, Lin Ye, Graham Clark, Yiu Wing Mai, Laser shock processing and its effects on microstructure and properties of metal alloys: a review, Int. J. Fatigue 24 (2002) 1021–1036.
[10] Harold Luong, Michael R. Hill, The effects of laser peening and shot peening on high cycle fatigue in 7050–T7451 aluminum alloy, Mater. Sci. Eng. A 527 (2010) 699–707.
[11] Abdullahi K. Gujba, Mamoun Medraj, Laser peening process and its impact on materials properties in comparison with shot peening and ultrasonic impact peening, Materials 7 (2014) 7925–7974.
[12] C. Rubio Gonzalez, J.L. Ocaña, G. Gomez Rosas, C. Molpeceres, M. Paredes, A. Banderas, J. Porro, M. Morales, Effect of laser shock processing on fatigue crack growth and fracture toughness of 6061–T6 aluminum alloy, Mater. Sci. Eng. A 386 (2004) 291–295.
[13] R. Fabbro, J. Fournier, P. Ballard, D. Devaux, J. Virmont, Physical study of laser produced plasma in confined geometry, J. Appl. Phys. 68 (1990) 775–784.
[14] Servando D. Cuellar, Michael R. Hill, Adrian T. Dewald, Jon E. Rankin, Residual stress and fatigue life in laser shock peened open hole samples, Int. J. Fatigue 44 (2012) 8–13.
[15] M. Achintha, D. Nowell, D. Fufari, E.E. Sackett, M.R. Bache, Fatigue behavior of geometric features subjected to laser shock peening: experiments and modeling, Int. J. Fatigue 62 (2014) 171–179.
[16] X.D. Ren, Q.B. Zhan, H.M. Yang, F.Z. Dai, C.Y. Cui, G.F. Sun, L. Ruan, The effects of residual stress on fatigue behavior and crack propagation from laser shock processing-worked hole, Mater. Des. 44 (2013) 149–154.
[17] X.D. Ren, Y.K. Zhang, H.F. Yongzhuo, L. Ruan, D.W. Jiang, T. Zhang, K.M. Chen, Effect of laser shock processing on the fatigue crack initiation and propagation of 7050–T7451 aluminum alloy, Mater. Sci. Eng. A 528 (2011) 2899–2903.
[18] Xing Quan Zhang, Liu San Chen, Xiao Liu Yu, Li Sheng Zuo, Yu Zhou, Effect of laser shock processing on fatigue life of fastener hole, Trans. Nonferr. Metals Soc. China 24 (2014) 969–974.

[19] Y.K. Zhang, J.Z. Lu, X.D. Ren, H.B. Yao, H.X. Yao, Effect of laser shock processing on the mechanical properties and fatigue lives of the turbojet engine blades manufactured by LY2 aluminum alloy, Mater. Des. 30 (2009) 1697–1703.
[20] X.Q. Zhang, H. Li, X.L. Yu, Y. Zhou, S.W. Duan, S.Z. Li, Z.L. Huang, L.S. Zuo, Investigation on effect of laser shock processing on fatigue crack initiation and its growth in aluminum alloy plate, Mater. Des. 65 (2015) 425–431.
[21] X.D. Ren, Y.K. Zhang, T. Zhang, D.W. Jiang, H.F. Yongzhuo, Y.F. Jiang, K.M. Chen, Comparison of the simulation and experimental fatigue crack behaviors in the nanoseconds laser shocked aluminum alloy, Mater. Des. 32 (2011) 1138–1143.
[22] Carlos Rubio-Gonzalez, G. Gomez-Rosas, R. Ruiz, M. Nait, A. Amrouche, Effect of laser shock peening and cold expansion on fatigue performance of open hole samples, Struct. Eng. Mech. 53 (2015) 867–880.
[23] Goran Ivetic, Ivan Meneghin, Enrico Troiani, Gianluca Molinari, Jose Ocaña, Miguel Morales, Juan Porro, Agostino Lanciotti, Vjola Ristori, Claudia Polese, Jasper Plaisier, Andrea Lausi, Fatigue in laser shock peened open-hole thin aluminum specimens, Mater. Sci. Eng. A 534 (2012) 573–579.
[24] C. Rubio Gonzalez, C. Felix Martinez, G. Gomez Rosas, J.L. Ocaña, M. Morales, J. A. Porro, Effect of laser shock processing on fatigue crack growth of duplex stainless steel, Mater. Sci. Eng. A 528 (2011) 914–919.
[25] Hyuntaeck Lim, Pilkyu Kim, Hoemin Jeong, Sungho Jeong, Enhancement of abrasion and corrosion resistance of duplex stainless steel by laser shock peening, J. Mater. Process. Technol. 212 (2012) 1347–1354.
[26] E. Castañeda, C. Rubio-Gonzalez, A. Chavez-Chavez, G. Gomez-Rosas, Laser shock processing with different conditions of treatment on duplex stainless steel, JMEPEG 24 (2015) 2521–2525.
[27] Hyuntaeck Lim, Myunghwa Lee, Pilkyu Kim, Jongbok Park, Sungho Jeong, Improvement of surface hardness of duplex stainless steel by laser shock hardening for the application to seawater desalination pump, Desalination Water Treat. 15 (2010) 43–47.
[28] ASTM International. E837-01 standard test method for determining residual stresses by the hole–drilling strain gage method. Annual book of ASTM Standards 2002; v.03.
[29] C. Rubio Gonzalez, G. Gomez-Rosas, J.L. Ocaña, C. Molpeceres, A. Banderas, J. Porro, M. Morales, Effect of an absorbent overlay on the residual stress field induced by laser shock processing on aluminum samples, Appl. Surf. Sci. 252 (2006) 6201–6205.
[30] Suvi Papula, Severi Anttila, Juho Talonen, Teemu Sarikka, Iikka Virkkunen, Hannu Hänninen, Strain hardening of cold-rolled lean-alloyed metastable ferritic-austenitic stainless steels, Mater. Sci. Eng. A 677 (2016) 11–19.
[31] S.K. Ghosh, D. Mahata, R. Roychaudhuri, R. Mondal, Effect of rolling deformation and solution treatment on microstructure and mechanical properties of a cast duplex stainless steel, Bull. Mater. Sci. 35 (2012) 839–846.
[32] M. De Giorg, Residual stress evolution in cold-rolled steels, Int. J. Fatigue 33 (2011) 507–512.
[33] C. Correa, D. Peral, J.A. Porro, M. Díaz, L. Ruiz de Lara, A. García-Beltrán, J.L. Ocaña, Random-type scanning patterns in laser shock peening without absorbing coating in 2024–T351 Al alloy: a solution to reduce residual stress anisotropy, Opt. Laser Technol. 73 (2015) 179–187.
[34] A. Salimianrizi, E. Foroozmehr, M. Badrossamay, H. Farrokhpour, Effect of Laser Shock Peening on surface properties and residual stress of Al6061-T6, Opt. Lasers Eng. 77 (2016) 112–117.
[35] E. Maawada, Y. Sano, L. Wagner, H.-G. Brokmeier, Ch. Genzel, Investigation of laser shock peening effects on residual stress state and fatigue performance of titanium alloys, Mater. Sci. Eng. A 536 (2012) 82–91.
[36] C. Correa, L. Ruiz de Lara, M. Diaz, A. Gil-Santos, J.A. Porro, J.L. Ocaña, Effect of advancing direction on fatigue life of 316L stainless steel specimens treated by double-sided laser shock peening, Int. J. Fatigue 79 (2015) 1–9.
[37] C. Correa, L. Ruiz de Lara, M. Díaz, J.A. Porro, A. García-Beltrán, J.L. Ocaña, Influence of pulse sequence and edge material effect on fatigue life of Al2024-T351 specimens treated by laser shock processing, Int. J. Fatigue 70 (2015) 196–204.
[38] Sagar Bhamare, Gokul Ramakrishnan, Seetha R. Mannava, Kristina Langer, Vijay K. Vasudevan, Dong Qian, Simulation-based optimization of laser shock peening process for improved bending fatigue life of Ti–6Al–2Sn–4Zr–2Mo alloy, Surf. Coat. Technol. 232 (2013) 464–474.
[39] R. Lillbacka, G. Chai, M. Ekh, P. Liu, E. Johnson, K. Runesson, Cyclic stress–strain behavior and load sharing in duplex stainless steels: aspects of modeling and experiments, Acta Material. 55 (2007) 5359–5368.
[40] X.Q. Zhang, H. Li, X.L. Yu, Y. Zhou, S.W. Duan, S.Z. Li, Investigation on effect of laser shock processing on fatigue crack initiation and its growth in aluminum alloy plate, Mater. Des. 65 (2015) 425–431.
[41] L. Zhang, J.Z. Lu, Y.K. Zhang, K.Y. Luo, J.W. Zhong, C.Y. Cui, Effects of different shocked paths on fatigue property of 7050–T7451 aluminum alloy during two-sided laser shock processing, Mater. Des. 32 (2011) 480–486.
[42] X.D. Ren, Q.B. Zhan, H.M. Yang, F.Z. Dai, C.Y. Cui, G.F. Sun, The effects of residual stress on fatigue behavior and crack propagation from laser shock processing-worked hole, Mater. Des. 44 (2013) 149–154.
[43] Q. Hongchao, Experimental investigation of laser peening on Ti17 titanium alloy for rotor blade applications, Appl. Surf. Sci. 351 (2015) 524–530.
[44] C. Rubio-González, A. Garnica-Guzmán, G. Gómez-Rosas, Relaxation of residual stresses induced by laser shock processing, Revista Mexicana de Física 55 (4) (2009) 256–261.